A NEW ALGORITHM TO GENERATE LOW-THRUST SPACECRAFT TRAJECTORIES

A Thesis by

Suwat Sreesawet

Bachelor of Engineering, Kasetsart University, 2009

Submitted to the Department of Aerospace Engineering
and the faculty of the Graduate School of
Wichita State University
in partial fulfillment of
the requirements for the degree of
Master of Science

December 2014

A NEW ALGORITHM TO GENERATE LOW-THRUST SPACECRAFT TRAJECTORIES

The following faculty members have examined the final copy of this thesis for form and content, and recommend that it be accepted in partial fulfillment of the requirement for the degree of Master of Science with a major in Aerospace Engineering.

_____
Atri Dutta, Committee Chair

_____
James E. Steck, Committee Member

_____
Animesh Chakravarthy, Committee Member

_____
John Watkins, Committee Member

ACKNOWLEDGMENTS

I would like to thank my adviser, Dr. Atri Dutta, for his guidance and support all along this thesis. I would also like to thank the committee members Dr. James E. Steck, Dr. John Watkins and Dr. Animesh Chakravarthy for their advice and suggestions for this research. I would also like to thank Ministry of Science and Technology, Thailand for funding my graduate program. Thanks also to my colleagues and friends who helped with their suggestions during the course of this project.

ABSTRACT

All-electric satellites are gaining favor among the manufacturers and operators of satellites in Geostationary Earth Orbit (GEO) due to cost saving potential. These satellites have the capability of performing all propulsive tasks with electric propulsion including transfer to GEO. Although fuel-efficient, electric thrusters lead to long transfer, during which the health and the usability of spacecraft is affected due to its exposure to hazardous space radiation in the Van Allen belts. Hence, determining electric orbit-raising trajectory that minimize transfer time is crucial for all-electric satellite operation.

This thesis proposes a novel method to determine minimum-time orbit-raising trajectory by blending the ideas of direct optimization and guidance-like trajectory optimization schemes. The proposed methodology is applicable for both planar and non-planar transfers and for transfers starting from arbitrary circular and elliptic orbits. Therefore, it can be used for rapidly analyzing various orbit-raising mission scenarios. The methodology utilizes the variational equations of motion of the satellite in the context of the two-body problem by considering the low-thrust of an electric engine as a perturbing force. The no-thrust condition due to Earth's shadow is also considered. The proposed methodology breaks the overall optimization problem into multiple sub-problems and each sub-problem minimizes a desired objective over the sun-lit part of the trajectory. Two different objective types are considered. Type *I* transfers minimize the deviation of the total energy and eccentricity of final position from the GEO, while type *II* transfers minimize the deviation of total energy and angular momentum. Using the developed tool, several mission scenarios are analyzed including, a new type of mission scenarios, in which more than one thruster type are used for the transfer. The thesis presents the result for all studied scenarios and compares the performance of Type *I* and Type *II* transfers.

TABLE OF CONTENTS

TABLE OF CONTENTS (continued)

Chapter Page

LIST OF TABLES

Table Page

LIST OF FIGURES

LIST OF FIGURES (continued)

Figure Page

NOMENCLATURE

Abbreviations

GEO	Geostationary Earth Orbit
GTO	Geostationary Transfer Orbit
IPOPT	Interior Point Optimizer
LEO	Low Earth Orbit
MPDT	Magnetoplasmadynamic Thruster
SNOPT	Sparse Nonlinear Optimizer
TPBVP	Two-Point Boundary-Value Problem

NOMENCLATURE (continued)

E	Specific Total Energy
e	Eccentricity
F	Force
G	Gravitational Constant (6.673×10^{-11} N(m/kg)^2)
h	Specific Angular Momentum
I_{sp}	Specific Impulse
m	Mass
m_{earth}	Mass of the Earth (5.971×10^{24} kg)
$m_{s/c}$	Mass of the Spacecraft
$\mathbf{h}$	Specific Angular Momentum Vector
h_{GEO}	Specific Angular Momentum of Geostationary Earth Orbit
$\mathbf{e}$	Eccentricity Vector
e_{GEO}	Eccentricity of Geostationary Earth Orbit
$\mathbf{r}$	Radius Vector
r_E	Radius of the Earth
t	Time
$\mathbf{T}$	Thrust
$\mathbf{v}$	Velocity
w	Weight Parameter
x, y, z	Cartesian Coordinates
$\dot{(\,)}$	Time Rate of Change

NOMENCLATURE (continued)

$\hat{(\ )}$	Unit Vector
$\tilde{(\ )}$	Approximated Quantity
$\bar{(\ )}$	Quantity at the End of a Revolution
$(\ )_r$	Vector in Direction of Radius Vector
$(\ )_n$	Vector in Direction of Local Horizon Vector
$(\ )_h$	Vector in Direction of Angular Momentum Vector

Greek Letters

α	Angle between Local Horizon and Projection of Thrust in Orbit on Orbit Plane
β	Angle between Thrust and Orbit Plane
γ	Flight Path Angle
μ	Earth Gravitational Constant
θ	True Anomaly Angle
$\boldsymbol{\omega}$	Angular Velocity Vector

CHAPTER 1

INTRODUCTION

Recently, the popularity of the all-electric satellites is growing among the satellites manufacturers and operators of telecommunication satellites. Boeing is manufacturing their 702-SP all-electric satellite bus architecture[1]. Several satellite operators, commercial and government, are also in the process of obtaining such satellites[2]. Other manufacturers are also in the process of developing such satellites. For these satellites, the electric thrusters perform all propulsive tasks including the transfer to the destination orbit which could be Geostationary Earth Orbit (GEO). Any object in GEO is always at the same point in the sky. The current practice is to use chemical propulsion for the orbit-raising maneuver after the satellites have been launched into their initial orbit by a launch vehicle. Usually, this initial orbit is a circular Low-Earth Orbit (LEO) with altitude less than 2000 km or an elliptical Geostationary Transfer Orbit (GTO) with periapsis altitude lower than 2000 km and apoapsis at the altitude of GEO. Due to the fuel-efficiency of electric thrusters (e.g. Hall or ion thrusters), the launch mass of the spacecraft could be significantly reduced by using electric thrusters for orbit-raising. The reduction of launch mass leads to smaller and lighter satellites that can either be launched by a smaller launch vehicle or can be stacked together in a larger launch vehicle. Obviously, electric orbit-raising have the potential of reducing the launch costs.

The focus of the current study is the orbit-raising maneuver of all-electric satellites. Although fuel-efficient, the orbital transfer using electric thrusters is a slow process because of the low thrust generated by electric thrusters. Except for MPDT that have extremely high power

[1] Source: http://www.boeing.com/boeing/defense-space/space/bss/factsheets/702/702SP.page
[2] Source: http://www.spacenews.com/article/satellite-telecom/39853news-from-satellite-2014-boeing-electric-satellite-backlog-poised-to

requirements, the thrust generated by an electric thruster is in the order of 100 mN, as shown in Table 1.1.

TABLE 1.1

REPRESENTATIVE OF ELECTRIC PROPULSION DEVICES [1]

Thruster	**Operating Principle**	**Operating Power (kW)**	**Thrust Generated (mN)**	**Specific Impulse (s)**	**Propellant**
Arcjet MR-510	Electrothermal	0.3-2	222-258	500-600	Hydrazine
Hall Thruster BPT-4000	Electrostatic	2.5-5.5	134-299	1700-2700	Xenon
Hall Thruster SPT-100B	Electrostatic	0.66-1.57	43.4-98.8	1600-2500	Xenon
Ion Thruster NSTAR	Electrostatic	0.5-2.3	19-92	1900-4000	Xenon
MPDT Li-LFA	Electromagnetic	30-200	10-12.5 $x10^3$	1500-8000	Lithium

The power available for today's telecom satellites is in the range of 5-20 kW. Hence, the solar array of telecommunication satellites can be used to operate multiple electric thrusters simultaneously in order to increase the amount of available thrust during the transfer. Even then, raising orbit to the GEO requires continuous thrusting for several months [1]. With this long period of time, it means that the spacecraft has to orbit around the Earth for numerous revolutions. The spacecraft would also pass through the shadow of the Earth for numerous times, once for each revolution. The presence of spacecraft in the eclipses mean that the solar panel cannot generate any power. Therefore, the scheme that thrusters are operated continuously is

impossible, unless the onboard energy storage is deployed. However, the onboard energy storage leads to an increase of spacecraft mass which partly negates the benefits of electric propulsion.

An area of energetically charged particles are found between the LEO and GEO, called Van Allen belts. The radiation belts are held in place by the Earth's magnetic field. Due to the proximity of this radiation belt to Earth, the spacecraft trajectories usually pass through this radiation area. The longer exposure to radiation from Van Allen belts leads to degradation of solar panels and is hazardous for other electronics. The minimum time transfer is useful in order to reduce the degradation from radiation. Therefore, the minimum transfer time is a crucial factor for orbit-raising mission analysis.

The transfer time depends on several factors. The first factor is the initial orbit where the spacecraft is initially launched by a suitable launch vehicle. Obviously, the closer initial orbit to GEO leads to smaller transfer time. Next, mass of the spacecraft also affects the transfer time. The heavier the spacecraft, the higher is the transfer time. Third, the electric engine uses solar array power to generate thrust. The capacity of solar array panels limit the number of thrusters in the spacecraft. The engine characteristics affects the thrust produced, which in turn affects the transfer time. The last one is the provision of battery which is used as the power sources of thruster during the eclipses. A mission designer needs to consider a variety of scenarios to understand the impact of the above factors. Due to these several factors, the tools that can evaluate the wide range of mission scenarios in an efficient way is necessary. Each mission scenario will require the determination of a minimum-time trajectory.

Determining a minimum-time trajectory requires solving an optimal control problem. In the next section, we present the existing methodologies of solving an optimal control problem.

1.1 Literature Survey

The trajectory optimization problem is a problem which relates to designing a trajectory that minimize or maximize an objective function. This function can be the transfer time, the final mass or solar array degradation along a path. Moreover, a solution trajectory must satisfy the equations of motion for the spacecraft.

The problem of low-thrust trajectory optimization have interested researchers for decades. Generally, there are primarily four different ways of generating optimal or near-optimal low-thrust trajectories: (1) Indirect optimization methods, (2) Direct optimization methods, (3) Shape-based methods and (4) Closed-loop guidance-like schemes. Each method has its own advantages and disadvantages. In this section, we provide an overview of the various methodologies.

1.1.1 Indirect Optimization Methods

Indirect optimization methods utilize the necessary conditions of optimality (obtained using calculus of variations [2-4]) to determine an optimal trajectory. The necessary conditions are usually a set of ordinary differential equations that need to be solved along with equations of motion which are also ordinary differential equations. The boundary conditions are known partly at initial time and partly at the final time; so this methodologies require the solution of a two-point boundary-value problem (TPBVP).

In 1996, Thorne and Hall [5] introduced the minimum time transfer for circular to circular orbit-raising by indirect optimization method. Their strategy was to repeatedly maximize the final radius for different flight times, then choosing the time such that the final radius is at the destination. Later in 1997, the same authors [6] extended the idea by introducing a transformation called “Kustaanheimo-Stiefel” in order to simplify the equation of motion in

planar orbit. Later in 2000, this transformation was also used by Marasch and Hall [7] in order to obtain low-thrust orbit-raising trajectories eclipse, with or without energy storage support.

1.1.2 Direct Optimization Methods

In the direct optimization methods, a trajectory optimization problem is converted into a parametric optimization problem by discretizing the time variable, the state and control variables. The equations of motion are assumed to hold only at the discretized modes; infact, the set of differential equations are converted to a bunch of algebraic equations that are the constraints for the parametric optimization problem. This problem is then solved using a non-linear programming solver like SNOPT® [8], IPOPT® [9] or LOQO® [10]. Hence, this methodology avoids the use of necessary condition of optimality; hence their name direct optimization. In comparison to indirect optimization method, this optimization method has the more tolerane of initial guesses and could converge to the solution better than indirect methods [3].

The coordinate system chosen to define the states affects the performance of this method because of the variation of state parameters. Since, these parameters are integrated stepwise by numerical integration technique, it does not yield accurate results if there is a rapid change in state parameters. One of implementation of direct optimization method for solving the minimum transfer time on spherical coordinates has been demonstrated by Dutta, et al. [1]. The direct optimization methods were also be implemented by Falck and Dankanich [11] in order to find an optimal solution for spiral trajectories on the costates of the classical or modified equinoctial orbital elements. Earlier in 2014, Libraro, et al. [12] presented the direct optimization for electric orbit-raising with a new state vector called quaternion-based formulation which is globally free of any singularity.

1.1.3 Shape-based methods

In the shape-based method, the spacecraft trajectory is assumed to be of a certain shape or geometric description. Then, the thrust profile that is required to generate that trajectory shape will be determined by satisfying the equation of motion along that trajectory. Shape-based methods aim at rapidly investigating the solution trajectory and provide a fast initial guess for the continuous-thrust trajectory [13] required for indirect and direct methods.

Some feasible trajectory shapes that have been investigated by researchers are the logarithmic spiral, Cartesian oval and Cassini oval [14]. As demonstrated by Petropoulos and Longuski [13] in 2004, the exponential sinusoid shapes in polar coordinates could be used to determine the Earth-Mars-Ceres rendezvous trajectories, and selected trajectories are successfully used as initial guess for the direct method optimization program. In 2006, De Pascale and Vasile introduced trajectory shapes based on non-singular equinoctial element, and could yield a good enough initial guess for direct and indirect methods [15]. In 2008, Wall [16] introduced a shape called inverse polynomial in cylindrical coordinates. Later in 2009, Wall and Conway [17] demonstrated the inverse polynomial shape in polar coordinates for efficient generation of near –optimal low-thrust trajectory. In 2011, Novak and Vasile [18] compared the exponential sinusoid shape in polar coordinates and equinoctial element based shapes. They found that the shaping method in polar coordinates provides better solutions than that in non-singular equinoctial coordinates. In 2012, finite Fourier series was used to approximate the trajectory shapes presented by Taheri and Abdelkhalik [19].

1.1.4 Closed-Loop Guidance-Like Schemes

Closed-loop guidance-like schemes aim to generate the low-thrust trajectory by using thrust profile based on some guidance law that minimizes the deviation of current trajectory from

the destination trajectory. Therefore, the solution trajectories are obtained by integrating these thrust profiles from the initial point till the end point.

In 1998, Kluever introduced a simple guidance scheme [20] that determines the thrust direction in order to maximize the time rate of change of a desired orbital element. The guidance scheme, therefore, determines the thrust direction which drives a desired orbital element to its target final value as fast as possible. The three orbital parameters considered are semi-major axis, eccentricity and inclination. The selected thrust direction is obtained by taking a weighted average of those directions. In 2003, Petropoulos introduced a new guidance scheme called "Q-Law" [21, 22]. The main concept is the evaluation of a "Proximity Quotient" that measures the proximity of current orbit and destination orbit. This method not only considered the maximum rate of change of orbital element at the current state like Kluever's scheme, but also considers over the whole state thereby including all orbital elements. The solutions generated are close to minimum-time solution.

These closed-loop guidance-like schemes have been implemented for achieving near optimal solutions without the need for frequent solution updates. Additionally, these could be used for robustly providing the solutions especially for the case of high disturbances which other methods could not be able to solve [23].

1.2 Research Objective and Thesis Contributions

The indirect and direct optimization methods still have the drawbacks that are the need of the reasonable initial guess and the lack of guarantees of convergences in the context of a tool for mission designers for all-electric satellite. These drawbacks lead to the limitations for rapidly investigating a wide range of scenarios, unlikely, the shape-based methods and closed-loop guidance-like schemes do not have these drawbacks and could be used to rapidly investigate a wide range of scenarios. However, that shape-based method is still complicated to determine the

initial shape, if it was implemented to solve all-electric orbit-raising to GEO problems. The reason is that low-thrust orbit-raising trajectories are usually spiral shapes with many revolutions (in the order of hundred/ thousands) which makes finding a shape satisfying equations of motion a challenging problem.

Closed-loop guidance-like schemes have the potential for use in a tool to rapidly investigate a wide range of scenarios. In this context, the thesis makes the following contributions:

1) A new formulation blending the ideas of direct optimization and guidance-like schemes.
2) Improvement over the work done by Marasch and Hall [7] by adding the capability of yielding the solution for non-planar cases, and non-circular initial orbit cases.
3) Improvement over Q-law in the sense that final orbit achieved is the GEO, owing to the non-singularity of the formulation.
4) Use of the tool in analyzing a new type of mission scenarios involving two different thruster types during transfer.

1.3 Thesis Organization

The thesis is organized as follows. Chapter 2 describes the spacecraft dynamics and the variational equation of motion. Chapter 3 describes the new optimization technique and strategy that have been used to determine low-thrust orbit-raising trajectories. The numerical method, which is used in implementation of those techniques, will be also described. In Chapter 4, the results of some examples would be demonstrated and discussed.

CHAPTER 2

MATHEMATICAL FORMULATION OF SPACECRAFT MOTION

Space mechanics is a science that describes the motion of objects in space including celestial bodies and spacecraft. A difference between a spacecraft and a natural body is that the spacecraft may apply its onboard propulsion system to alter its trajectory. In general, space is a multi-body environment, but in the context of electric orbit-raising mission, we will only consider two bodies, Earth and the spacecraft.

2.1 Two-Body Equation of Motion

The starting point of two-body problem is the Newton's law of gravitation which describes the attractive forces between the two masses. In the case of orbiting spacecraft around the Earth, the first assumption is that there are only two bodies under consideration. This assumption is good for planetary missions and the effects of other bodies can be modeled as a perturbation. Another assumption is that all objects are point masses. This second assumption works properly for spherical objects of uniform mass distribution. However, the impact of having a non-spherical body can also be modeled as a perturbation, for instance, J_2 effect of Earth [24].

The motion of the spacecraft relative to the Earth can be described by the following equation of motion (for the 2-body problem):

$$\ddot{\mathbf{r}} = -\frac{G(m_{earth} + m_{s/c})}{r^3}\mathbf{r} \tag{2.1}$$

where $\mathbf{r}$ is the radius vector from Earth to spacecraft, G is gravitational constant, m_{earth} is mass of the Earth and $m_{s/c}$ is mass of the spacecraft. The parameter μ is used for $G(m_{earth} + m_{s/c})$ and then equation (2.1) becomes:

$$\ddot{\mathbf{r}} = -\frac{\mu}{r^3}\mathbf{r} \tag{2.2}$$

The mass of the Earth is much larger than the typical spacecraft mass, so that one can approximate μ by Gm_{earth}, which is equal to 3.986×10^5 km^{3}s^{-2}. Equation (2.2) can be used to describe the motion of spacecraft as long as there is no other force than the mutual gravitational force. The constants of motion for the 2-body problem, henceforth referred to as dynamical quantities, are specific total energy, specific angular momentum vector and eccentricity vector.

2.1.1 Specific Total Energy

The specific total energy (E) is the total mechanical energy of spacecraft per unit mass, and is given by [24]:

$$E = \frac{v^2}{2} - \frac{\mu}{r} \tag{2.3}$$

where v is velocity of the spacecraft. In addition, equation (2.3) is comprised of two terms adding together, the kinetic energy per unit mass ($v^2/2$) and potential energy per unit mass ($-\mu/r$). The potential energy per unit mass term is set to be zero at the infinity as the reference point. So it will be more negative as it moves closer to the center of the Earth and never be positive. In this thesis, this specific total energy will henceforth be stated only as total energy, with the term "specific" dropped out.

2.1.2 Specific Angular Momentum Vector

The specific angular momentum ($\mathbf{h}$) is the angular momentum per unit of mass. It is simply defined as [24]:

$$\mathbf{h} = \mathbf{r}\times\dot{\mathbf{r}} = \mathbf{r}\times\mathbf{v} \tag{2.4}$$

By definition, its direction is always perpendicular to the orbital plane in which the 2-body motion is constrained. Hence, angular momentum provides the information about the orientation of the orbit plane. Later in this thesis, this specific angular momentum would be stated only as angular momentum.

2.1.3 Eccentricity Vector

Eccentricity $\mathbf{e}$ is a vector that points from the center of the central body to the point of closest approach (periapsis) of an orbit to the central body. The eccentricity vector of an orbit is defined as:

$$\mathbf{e} = \frac{\mathbf{v} \times \mathbf{h}}{\mu} - \frac{\mathbf{r}}{r} \tag{2.5}$$

In addition, its magnitude also provides information about the shape of an orbit. Depending on the eccentricity value, an orbit can be a circle, ellipse, parabola or a hyperbola.

2.2 Solutions to the Two-Body Problem

The motion of spacecraft which are governed by equation (2.2) can be categorized into 4 types based on the initial radius vector and velocity vector. All of these types are the conic sections which are parabola, circle, ellipse and hyperbola as shown in Figure 2.1. The conic sections represent the shape of spacecraft trajectory or spacecraft orbits. The total energy and eccentricity give the information to determine the type of the orbit. The summarized characteristic of four different orbit types in terms of total energy and eccentricity is shown in Table 2.1.

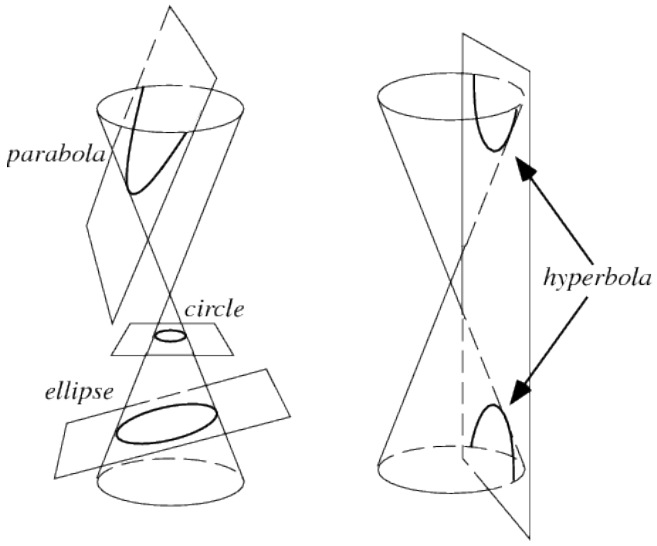

Figure 2.1 Types of conic sections

TABLE 2.1

CHARACTERISTIC OF FOUR DIFFERENT ORBIT TYPES

Orbit Type	Circular	Elliptic	Parabolic	Hyperbolic
Total Energy (E)	$E<0$	$E<0$	$E=0$	$E>0$
Eccentricity (e)	$e=0$	$0<e<1$	$e=1$	$e>1$

Additionally, there are other orbits which $e=1$ and its angular momentum is always zero because its radius vector and velocity vector is always perpendicular.

There are three other quantities related to an orbit, which will be mentioned later. These quantities are needed to be discussed. The first is flight path angle (γ). The second is radius-sweeping area per time unit. The last is true anomaly angle (θ).

2.2.1 Flight Path Angle

Flight path angle (γ) is a scalar quantity that defines the angle between local horizon direction and the velocity vector by measuring positively outward to the orbit as shown in Figure 2.2

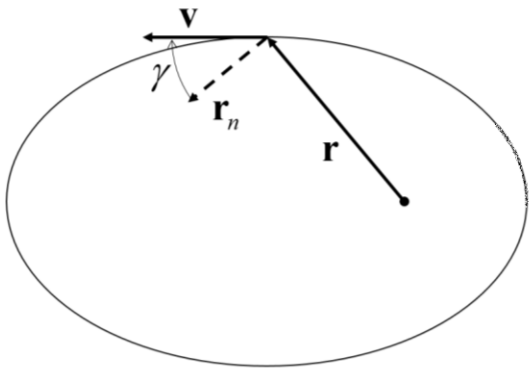

Figure 2.2 Description of flight path angle

This quantity can be computed by considering the magnitude of angular momentum as below.

$$h = rv\cos\gamma \tag{2.6}$$

Then, flight path angle is calculated by:

$$\gamma = \cos^{-1}(\frac{rv}{h}) \tag{2.7}$$

2.2.2 Radius-Sweeping Area per Time

First of all, consider the differential area of triangle that swept by the radius as shown in Figure 2.3.

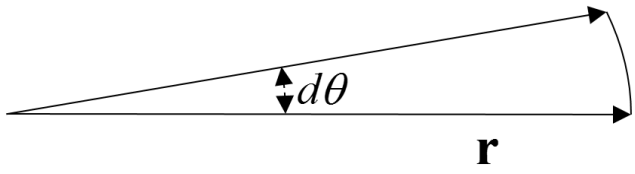

Figure 2.3 Triangle from sweeping radius

The differential area can be written as follows:

$$dA = \frac{1}{2} r \left(r d\theta \right) \tag{2.8}$$

Where dA is the differential area, r is radius which is the length of a triangle edge, $d\theta$ is the differential angle of the area. This differential angle $d\theta$ can be written in term of angular velocity and differential time interval as below

$$d\theta = \dot{\theta} dt \tag{2.9}$$

Substituting equation (2.9) into equation (2.8) lead to:

$$\frac{dA}{dt} = \frac{1}{2} r \left(r\dot{\theta} \right) \tag{2.10}$$

Noting that radius times angular velocity is equal to tangential velocity which is equal to $v \cos\gamma$. Then equation (2.10) can be rewritten as below:

$$\frac{dA}{dt} = \frac{1}{2} r \left(v \cos\gamma \right) = \frac{1}{2} h \tag{2.11}$$

The equation (2.11) gives the relationship of the area which is swept by radius vector per time unit and angular momentum. Finally, the differential time of flight is stated as:

$$dt = \frac{2dA}{h} \tag{2.12}$$

2.2.3 True Anomaly Angle

True anomaly angle (θ) is the angle measured from periapsis to radius vector in the direction of spacecraft orbital motion. So it is between 0 to 2π . The relation between true anomaly and radius is shown as below [24]:

$$r = \frac{h^2}{\mu(1 + e\cos\theta)} \tag{2.13}$$

Since,

$$e = \sqrt{1 + \frac{2Eh^2}{\mu^2}} \tag{2.14}$$

Then, substitution equation (2.14) into equation (2.13) lead to

$$r = \frac{h^2}{\mu + \sqrt{\mu^2 + 2Eh^2}\cos\theta} \tag{2.15}$$

2.3 Spacecraft Motion under Perturbing Forces

Because the thrust provided by all-electric satellites is small, the thrust acceleration is much small compared to the local gravitational acceleration. Hence, the thrust force can be viewed as a perturbing force. Under the action of a perturbing force, there are slow changes in the orbital parameters and in the dynamical quantities of interest. In the presence of other forces such as thrust, the equation (2.2) is modified into as below:

$$\ddot{\mathbf{r}} = -\frac{\mu}{r^3}\mathbf{r} + \frac{\mathbf{F}}{m} \tag{2.16}$$

where $\mathbf{F}$ is force vector or perturbation vector and m is mass of the spacecraft. Equation (2.16) can explicitly be written in Cartesian coordinates as follows

$$\dot{r}_x = v_x \tag{2.17}$$

$$\dot{r}_y = v_y \tag{2.18}$$

$$\dot{r}_z = v_z \tag{2.19}$$

$$\dot{v}_x = -\frac{\mu}{r^3} r_x + \frac{F_x}{m} \tag{2.20}$$

$$\dot{v}_y = -\frac{\mu}{r^3} r_y + \frac{F_y}{m} \tag{2.21}$$

$$\dot{v}_z = -\frac{\mu}{r^3} r_z + \frac{F_z}{m} \tag{2.22}$$

where r_x, r_y, r_z are the radius components in x, y, z axis, respectively. v_x, v_y, v_z are the velocity components and F_x, F_y, F_z are the perturbation forces in x, y, z axis, respectively. The presence of other forces imply that the dynamical quantities are no longer constants and their variations will be discussed in the next section. The spacecraft can be transferred to the destination orbit by this perturbation force which is controlled thrust. The example of continuous low-thrust orbit-raising is shown in Figure 2.4 by starting at an elliptical orbit on equatorial plane with 5000 km perigee altitude and 10000 km apogee altitude. The initial mass of spacecraft is 5000 kg. The perturbation force is engine thrust generated by four Hall thrusters, so that thrust is 1.16 N with specific impulse of 1788 s and is in the local horizon for a hundred days, so this is a case of planar transfer to GEO. Obviously from the figure, the spacecraft moves in spiral shape around the Earth for many revolutions and gradually increases its altitude.

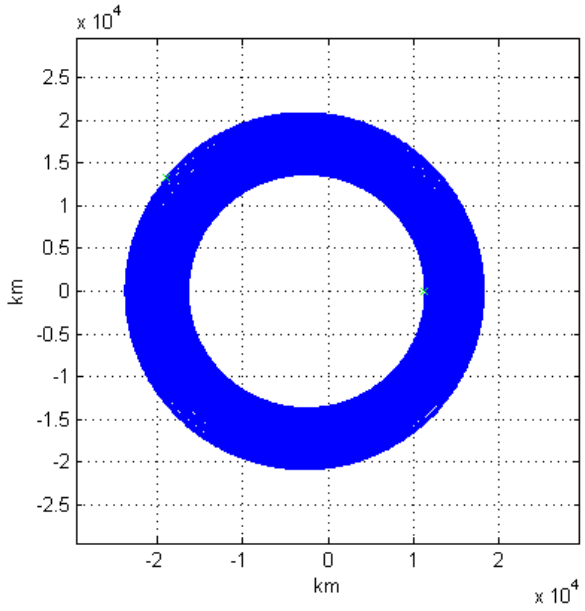

Figure 2.4 Example of low-thrust trajectory of a planar case

2.3.1 Variation of Total Energy

Naturally, the total energy will be constant as long as there is no existing perturbation forces. However, in the presence of the perturbation forces, the total energy will change. In order to transfer the spacecraft into destination orbit, the total energy is driven to the value at the destination orbit. So, the variation of total energy due to the perturbation forces has to be considered. Its time rate of change could be computed by taking the dot product of velocity vector on both sides of equation (2.16).

$$\dot{\mathbf{r}} \cdot \ddot{\mathbf{r}} = \dot{\mathbf{r}} \cdot \left(\frac{-\mu}{r^3}\mathbf{r} + \frac{\mathbf{F}}{m}\right) \tag{2.23}$$

Consider the left hand side of equation (2.23). From the chain rule of derivatives,

$$\dot{\mathbf{r}} \cdot \ddot{\mathbf{r}} = \frac{d}{dt}\left(\frac{1}{2}\dot{\mathbf{r}} \cdot \dot{\mathbf{r}}\right) \quad \text{or} \quad \dot{\mathbf{r}} \cdot \ddot{\mathbf{r}} = \frac{d}{dt}\left(\frac{1}{2}v^2\right) \tag{2.24}$$

Then, consider the right hand side of equation (2.23), there is a term ($\dot{\mathbf{r}} \cdot \mathbf{r}$). The term time rate of change of radius unit vector ($\dot{\hat{\mathbf{r}}}$) is perpendicular to $\mathbf{r}$, because the rate of change of unit vector

has to be perpendicular to unit vector itself in order to keep the magnitude at unity. So $\dot{\mathbf{r}} \times \mathbf{r}$ is equal to 0. Then one can show that:

$$\dot{\mathbf{r}} \cdot \mathbf{r} = \frac{d}{dt}(r\hat{\mathbf{r}}) \cdot \mathbf{r} = \left(\dot{r}\hat{\mathbf{r}} + r\dot{\hat{\mathbf{r}}}\right) \cdot \mathbf{r} = r\dot{r} \tag{2.25}$$

Then, multiply equation (2.25) by the term ($-\mu/r^3$):

$$\frac{-\mu}{r^3}\left(\dot{\mathbf{r}} \cdot \mathbf{r}\right) = \frac{-\mu}{r^3}\left(r\dot{r}\right) = \frac{-\mu\dot{r}}{r^2} = \frac{d}{dt}\left(\frac{\mu}{r}\right) \tag{2.26}$$

Substitute equation (2.24) and equation (2.26) into equation (2.23):

$$\frac{d}{dt}\left(\frac{1}{2}v^2\right) = \frac{d}{dt}\left(\frac{\mu}{r}\right) + \frac{\mathbf{F} \cdot \dot{\mathbf{r}}}{m} \tag{2.27}$$

Adjust equation (2.27) and compare with equation (2.3).

$$\frac{d}{dt}\left(\frac{1}{2}v^2\right) - \frac{d}{dt}\left(\frac{\mu}{r}\right) = \frac{d}{dt}\left(\frac{1}{2}v^2 - \frac{\mu}{r}\right) = +\frac{\mathbf{F} \cdot \dot{\mathbf{r}}}{m} \tag{2.28}$$

$$\dot{E} = \frac{\mathbf{F} \cdot \dot{\mathbf{r}}}{m} \tag{2.29}$$

The time variation of total energy is shown as stated in equation (2.29).

2.3.2 Variation of Angular Momentum Vector

The angular momentum vector is also a constant as long as the perturbations do not exist. This dynamical quantity also has to be driven to the value of destination orbit. If the perturbation forces exist, its variation due to the perturbations can be computed by taking the cross product of radius vector into both side of equation (2.16).

$$\mathbf{r} \times \ddot{\mathbf{r}} = \mathbf{r} \times \left(\frac{-\mu}{r^3}\mathbf{r} + \frac{\mathbf{F}}{m}\right) \tag{2.30}$$

Based on the chain rule for derivatives, an equation can be stated as below:

$$\frac{d}{dt}\left(\mathbf{r} \times \dot{\mathbf{r}}\right) = \left(\dot{\mathbf{r}} \times \dot{\mathbf{r}}\right) + \left(\mathbf{r} \times \ddot{\mathbf{r}}\right) = \mathbf{r} \times \ddot{\mathbf{r}} \tag{2.31}$$

Substitute the term ($\boldsymbol{r}\times\ddot{\boldsymbol{r}}$) on the left hand side of equation (2.30) by equation (2.31) and note that vectors cross into itself is equal to zero.

$$\frac{d}{dt}\left(\mathbf{r}\times\dot{\mathbf{r}}\right)=\mathbf{r}\times\frac{\mathbf{F}}{m} \tag{2.32}$$

Substituting equation (2.4) into equation (2.32) leads to:

$$\dot{\mathbf{h}}=\mathbf{r}\times\frac{\mathbf{F}}{m} \tag{2.33}$$

The equation (2.33) stated the variation of angular momentum vector which is the combination of the rate of its magnitude and its direction. Therefore, an equation is formed as below:

$$\dot{\mathbf{h}}=\mathbf{r}\times\frac{\mathbf{F}}{m}=\dot{h}\hat{\mathbf{h}}+\left(\boldsymbol{\omega}\times\mathbf{h}\right) \tag{2.34}$$

where $\boldsymbol{\omega}$ is angular velocity vector that the vector ($\mathbf{h}$) rotates through the space. Then, let us consider if perturbation force vector ($\mathbf{F}$) and other vectors in equation (2.26) are defined on the coordinates of radius vector ($\hat{\mathbf{r}}$), local horizontal ($\hat{\mathbf{r}}_{\mathbf{n}}$) and angular momentum ($\hat{\mathbf{h}}$) which are related as $\hat{\mathbf{r}}\times\hat{\mathbf{r}}_{\mathbf{n}}=\hat{\mathbf{h}}$, then equation (2.34) can be rewritten. Noting that $\boldsymbol{\omega}$ by definition is always perpendicular to h, so there is no component of $\boldsymbol{\omega}$ along $\mathbf{h}$:

$$r\hat{\mathbf{r}}\times\frac{\left(F_r\hat{\mathbf{r}}+F_n\hat{\mathbf{r}}_{\mathbf{n}}+F_h\hat{\mathbf{h}}\right)}{m}=\dot{h}\hat{\mathbf{h}}+\left(\left(\omega_r\hat{\mathbf{r}}+\omega_n\hat{\mathbf{r}}_{\mathbf{n}}\right)\times h\hat{\mathbf{h}}\right) \tag{2.35}$$

Simplifying the equation (2.35) results as:

$$\frac{rF_n}{m}\hat{\mathbf{h}}-\frac{rF_h}{m}\hat{\mathbf{r}}_{\mathbf{n}}=\dot{h}\hat{\mathbf{h}}+\omega_n h\hat{\mathbf{r}}-\omega_r h\hat{\mathbf{r}}_n \tag{2.36}$$

Comparisons of equation (2.36) along each direction result as:

$$\dot{h}=\frac{rF_n}{m} \tag{2.37}$$

$$\omega_n=0 \tag{2.38}$$

$$\omega_r = \frac{rF_h}{mh} \tag{2.39}$$

Equation (2.37), which is the result of comparison along $\hat{\mathbf{h}}$, can be considered as the description of the variation of angular momentum magnitude. As comparisons along $\hat{\mathbf{r}}$ and $\hat{\mathbf{r}}_n$ are resulting equation (2.38) and equation (2.39) respectively, $\boldsymbol{\omega}$ has only one component along $\hat{\mathbf{r}}$. Therefore, $\boldsymbol{\omega}$ can be stated as follows:

$$\boldsymbol{\omega} = \frac{rF_h}{mh}\hat{\mathbf{r}} \tag{2.40}$$

From the equation (2.40), the rotation of angular momentum is described by the right-hand rule which angular momentum rotates about radius due to the perturbation along $\hat{\mathbf{h}}$. As shown in the Figure 2.5, the thrust along angular momentum does not change the magnitude of angular momentum. However it changes the direction of angular momentum by rotating about radius vector as dash vector shown in Figure 2.5. The dash orbit in Figure 2.5 shows the corresponding change in terms of orbital orientation due to the thrust.

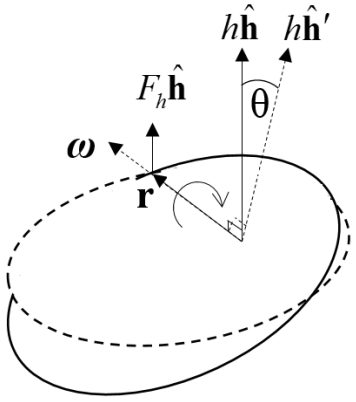

Figure 2.5 The rotation direction of angular momentum vector

2.3.3 Variation of Eccentricity Vector

In the case that the perturbation exists, the eccentricity is also changed. Its variation could be calculate by cross product of $\mathbf{h}$ into equation (2.16)

$$\ddot{\mathbf{r}}\times\mathbf{h}=(\frac{-\mu}{r^3}\mathbf{r}+\frac{\mathbf{F}}{m})\times\mathbf{h}=\frac{-\mu}{r^3}(\mathbf{r}\times\mathbf{h})+\frac{1}{m}(\mathbf{F}\times\mathbf{h}) \tag{2.41}$$

From the chain rule of derivatives:

$$\frac{d}{dt}(\dot{\mathbf{r}}\times\mathbf{h})=(\ddot{\mathbf{r}}\times\mathbf{h})+(\dot{\mathbf{r}}\times\dot{\mathbf{h}}) \tag{2.42}$$

Adjusting equation (2.42) lead to:

$$(\ddot{\mathbf{r}}\times\mathbf{h})=\frac{d}{dt}(\dot{\mathbf{r}}\times\mathbf{h})-(\dot{\mathbf{r}}\times\dot{\mathbf{h}}) \tag{2.43}$$

Consider the term ($\mathbf{r}\times\mathbf{h}$) which is on the right hand side of equation (2.41). From Equation (2.4) and vector triple product rule, this term becomes:

$$\mathbf{r}\times\mathbf{h}=\mathbf{r}\times(\mathbf{r}\times\dot{\mathbf{r}})=(\mathbf{r}\cdot\dot{\mathbf{r}})\mathbf{r}-(\mathbf{r}\cdot\mathbf{r})\dot{\mathbf{r}} \tag{2.44}$$

From equation (2.25) and that $\mathbf{r}$ dot product into itself is equal to r^2, the equation (2.44) can be written as:

$$\mathbf{r}\times\mathbf{h}=(r\dot{r})\mathbf{r}-(r^2)\dot{\mathbf{r}} \tag{2.45}$$

Multiplying equation (2.45) by $-\mu/r^3$ and using chain rule for derivatives:

$$\frac{-\mu}{r^3}(\mathbf{r}\times\mathbf{h})=-\left(\frac{\mu\dot{r}}{r^2}\right)\mathbf{r}+(r^2)\dot{\mathbf{r}} \tag{2.46}$$

$$\frac{-\mu}{r^3}(\mathbf{r}\times\mathbf{h})=\frac{d}{dt}\left(\frac{\mu}{r}\mathbf{r}\right) \tag{2.47}$$

Substitution of equation (2.43) and equation (2.47) into equation (2.41) leads to:

$$\frac{d}{dt}(\dot{\mathbf{r}}\times\mathbf{h})-(\dot{\mathbf{r}}\times\dot{\mathbf{h}})=\frac{d}{dt}\left(\frac{\mu}{r}\mathbf{r}\right)+\frac{1}{m}(\mathbf{F}\times\mathbf{h}) \tag{2.48}$$

Adjusting the equation (2.48) results as:

$$\frac{d}{dt}\left(\frac{\dot{\mathbf{r}}\times\mathbf{h}}{\mu}-\frac{\mathbf{r}}{r}\right)=\frac{1}{\mu}\left(\mathbf{v}\times\dot{\mathbf{h}}\right)+\frac{1}{\mu m}\left(\mathbf{F}\times\mathbf{h}\right) \tag{2.49}$$

Substituting equation (2.5) and equation (2.33) into equation (2.49) leads to:

$$\dot{\mathbf{e}}=\frac{1}{\mu m}\left[\left(\mathbf{v}\times\mathbf{r}\times\mathbf{F}\right)+\left(\mathbf{F}\times\mathbf{h}\right)\right] \tag{2.50}$$

These variations of dynamical quantities constitute the variational equations of motion for the spacecraft. In the next chapter, the demonstration of using these equation in the context of trajectory optimization are discussed.

CHAPTER 3

PROBLEM DESCRIPTION AND SOLUTION METHOD

As mentioned earlier about the benefits of all-electric orbit raising, the problem in this research is the minimum-time transfer for deploying electric thrusters from LEO or GTO to GEO by. In this chapter, the detail of problem is discussed and the method which is used to solve the problem is also explained.

3.1 Problem Descriptions

The information related to the problem is given in this section including the GEO, the electric thruster and model of the eclipse.

3.1.1 Geostationary Earth Orbit

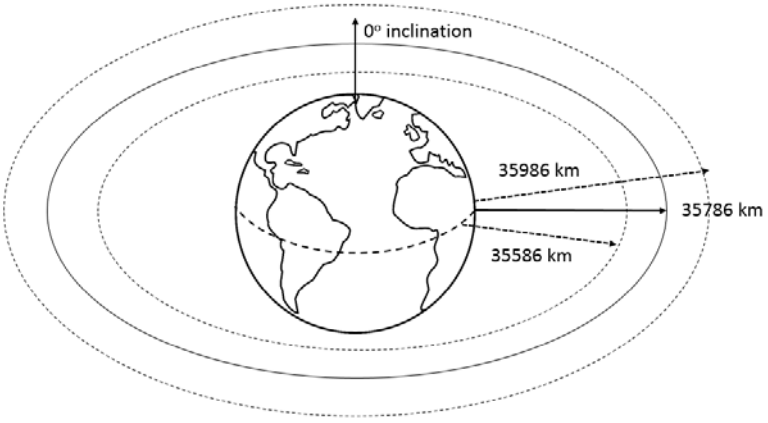

Figure 3.1 Graphical explanation of GEO (Not to Scale)

GEO is a circular orbit around the Earth in the equatorial plane. Its orbital period is one sidereal day matching with Earth rotation period. The observers on the surface of the Earth would found that any object in this orbit is always at the same point in the sky. The satellite antennas that communicate with them can be permanently fixed to a satellite location in the sky.

In a technical term, the GEO is defined by Inter-Agency Space Debris Coordination [25] (IADC) as a circular orbit which has altitude 35786 km with 0 degree inclination. In addition, GEO region is also defined by IADC as lower altitude and upper altitude are equal to GEO altitude minus 200 km and plus 200 km, respectively. Then, the graphical explanation of GEO is shown in Figure 3.1. From this definition, we can further compute the other quantity of GEO region for obtaining result as below:

$$a_{GEO,\min} = 41964 \quad \text{to} \quad a_{GEO,\max} = 42364 \qquad \text{km} \qquad (3.1)$$

$$e_{GEO,\min} = 0 \quad \text{to} \quad e_{GEO,\max} = 0.004743 \qquad (3.2)$$

$$E_{GEO,\min} = -4.7493 \quad \text{to} \quad E_{GEO,\max} = -4.7045 \qquad \text{km}^2/\text{s}^2 \qquad (3.3)$$

$$h_{GEO,\min} = 129332 \quad \text{to} \quad h_{GEO,\max} = 129947 \qquad \text{km}^2/\text{s} \qquad (3.4)$$

As the consequences of being circular orbit, GEO has no periapsis or apoapsis. GEO can be completely defined by only the pair of total energy and angular momentum.

3.1.2 Electric Thruster

Thrust, force generated by the engines, will be defined by 3 parameters. The first parameter is the magnitude of the thrust (T). The direction of thrust is defined by 2 angles, one in the orbit plane (α) and the other out-of-the plane (β). α is measured from the local horizon vector and is consider to be positive if it rotates into the central body. And, β is measured from the orbital plane and is considered to be positive if it tilts into angular momentum vector as shown in Figure 3.2.

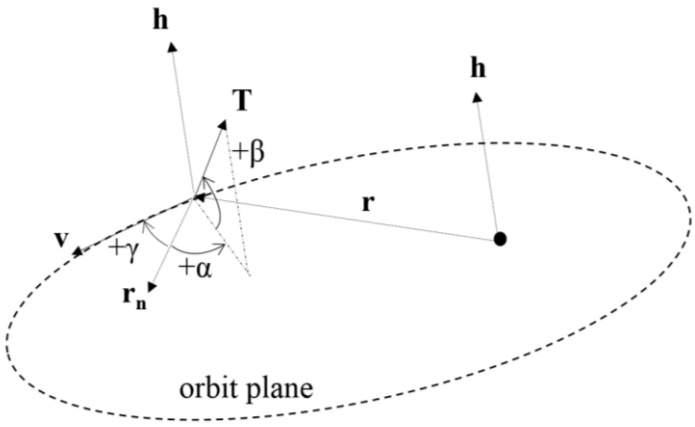

Figure 3.2 Definition of Thrust Vector

Specific impulse (I_{sp}) is the characteristic of engines. This parameter is related to the rate of change of fuel mass. The relation is given by:

$$\dot{m} = -\frac{T}{g_0 I_{sp}} \tag{3.5}$$

where g_0 is gravitational acceleration at surface of the earth which is 9.81 m/s^2.

3.1.3 Modeling Shadow of the Earth

When the satellite moves into the eclipse, there will be lack of the power to provide to the engine unless deploying the other power storages. In the methodology presented in this thesis, the thrust is assumed to be zero, if the satellite moves into eclipses. The shadow geometry is assumed to be cylindrical with its length stretching to infinity pointing from the center of the Earth in the direction opposite to the sun and with the radius equal to the radius of the Earth as shown in Figure 3.3. In the Figure 3.3, the sun is assumed to lie on the negative side of x-axis, so the eclipses are stretching from the origin into positive infinity of x-axis with radius equal to radius of the Earth. Furthermore, the position of the sun in this problem is assumed to be stationary, thus eclipse geometry do not change over time. In reality, the eclipse orientation

changes as the Earth revolves round the Sun in its orbit; however, we neglect this variation in the thesis.

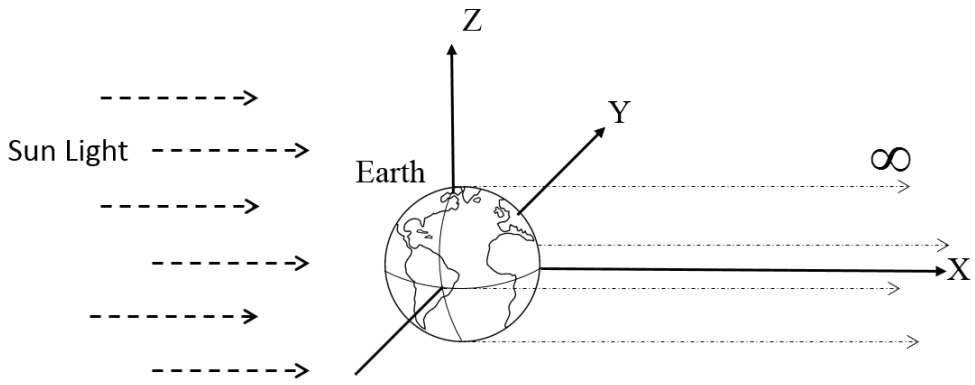

Figure 3.3 Shadow geometry stretching to infinity

We can, therefore, form the conditions which can be used to specify the presence of spacecraft in the shadow of the Earth in Cartesian coordinates as follows:

$$x > 0 \quad \text{and} \quad \sqrt{y^2 + z^2} < r_E \tag{3.6}$$

where r_E is the radius of the Earth. When the satellites move into the eclipse, there will be lack of power to provide to the engine unless onboard batteries are used because the solar panel cannot generate the power for the engines to operate. The satellite has no onboard batteries. Then, the condition in equation (3.6) can be stated as below:

$$T = \begin{cases} 0, & if \quad x > 0 \quad and \quad \sqrt{y^2 + z^2} < r \\ T_{\max}, & \text{otherwise} \end{cases} \tag{3.7}$$

where $T_{\max}$ is maximum thrust. For examples of orbit-raising with eclipse consideration, the trajectories are shown in Figure 3.4. On the left of Figure 3.4, the initial orbit is 5000 km periapsis altitude and 15000 km apoapsis altitude, and on the right the initial orbit is circular orbit with 5000 km altitude. For both cases, thrust is generated by four Hall thrusters in local

horizon direction, so maximum thrust is 1.16 N with specific impulse of 1788 s. Initial mass is 5000 kg for both cases.

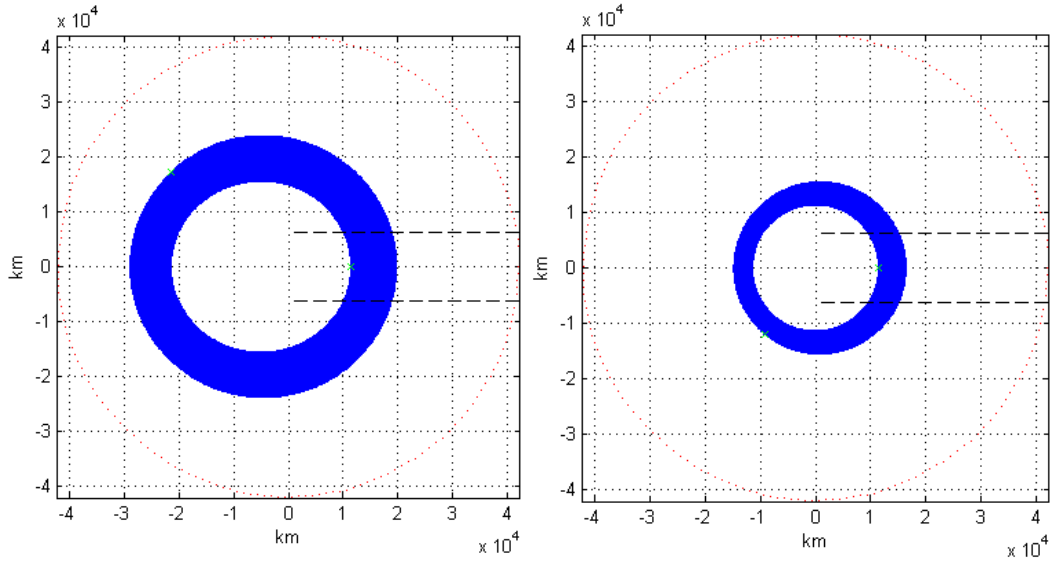

Figure 3.4 Trajectories of elliptical orbit (left) and circular orbit (right) with absence of thrust in eclipse which is the dash line

3.2 Methodology

A new methodology is developed in this thesis to determine the low-thrust trajectories in eclipses. As mentioned before, this methodology brings together the ideas of direct optimization and guidance-like schemes. More specifically, the methodology improves upon the work of Marasch and Hall [7] to determine the low-thrust trajectory in eclipses starting from arbitrary orbits.

3.2.1 Concepts of Methodology and Assumption

There are two main concepts for this methodology. The first concept comes from Marash and Hall [7] which is that break the problem into optimization over a single revolution sub-

problems, each. The second concept comes from the closed-loop guidance scheme which that reducing the deviation between current state and destination state as fast as possible.

Three assumptions are made for simplifying the problem. The first assumption is that the shape of an orbit are not changed during a revolution. The second assumption is that the projection of vector that points to apsis on the equatorial plane does not rotate for the entire trajectory and lies on x-axis as well as angular momentum. This assumption comes from the observation the solutions of electric-orbit raising to GEO problem [21, 22] that the direction of apsis do not change significantly. The third assumption is that the angle that angular momentum direction changes in each revolution is small. This assumption leads to that the rotation of angular momentum vector can be considered as infinitesimal rotations. The angle rotated can be considered as a vector [26].

3.2.2 Objective Function

In order to achieve research objectives, the closed-loop guidance-like schemes is selected as discussed earlier in Chapter 1. In the literature [20-22], this kind of methodology solves the minimum transfer time problem by aiming to reduce the gap between current orbit and destination orbit as fast as possible. Then, the thrust profiles are determined based on this concept. In other words, the solution is the thrust profiles that satisfies objective function stated below:

$$\min\left[\sum_{j\in N} w_j \left(P_{j,GEO} - \widehat{P}_j\right)^2\right] \tag{3.8}$$

where N is the number of orbital parameters which is used to defined the GEO, w_j is the weight parameter for each dynamical quantity, $P_{j,\mathrm{GEO}}$ is the value of each dynamical quantity at the GEO, $\widehat{P}_j$ is the value of each dynamical quantity at the end of current revolution.

A. Planar Case

In this case, the orientation of the orbit is not considered. Then, GEO can be defined by a pair of dynamical quantities which are described earlier. We consider two different objective functions Type *I* and Type *II*. For Type I, a pair of total energy and eccentricity is selected, so the objective function in equation (3.8) can be rewritten as follows:

$$\min\left[w_1 \left(e_{GEO} - \hat{e}\right)^2 + w_2 \left(E_{GEO} - \hat{E}\right)^2 \right] \tag{3.9}$$

where $\hat{e}$ and $\hat{E}$ are the eccentricity and total energy at the end of current revolution.

For Type *II*, a pair of angular momentum and total energy is chosen, then the objective function in equation (3.8) is rewritten as follow:

$$\min\left[w_1 \left(h_{GEO} - \hat{h}\right)^2 + w_2 \left(E_{GEO} - \hat{E}\right)^2 \right] \tag{3.10}$$

B. Non-Planar Case

In this case the orientation of trajectory has to be considered. The angular momentum of current orbit is needed to be aligned with z axis. In order to measure the deviation in terms of orientation from destination, we define a new vector ($\boldsymbol{I}$) on the orbit plane. The magnitude of this vector is equal to the inclination angle of the orbit which is in between 0 to 2π . And the direction of this is along the direction of angular velocity on the orbit plane which rotates the angular momentum into z axis. The graphical definition of vector is depicted in Figure 3.5. Therefore, from the definition given, the magnitude of this vector can be computed as follows

$$I = \left|\mathbf{I}\right| = \cos^{-1}(\hat{\mathbf{h}} \cdot \hat{\mathbf{k}}) \tag{3.11}$$

where $\hat{\mathbf{k}}$ is a unit vector along z axis. And its direction is computed by

$$\hat{\mathbf{I}} = \frac{\hat{\mathbf{h}} \times \hat{\mathbf{k}}}{\left| \hat{\mathbf{h}} \times \hat{\mathbf{k}} \right|} \tag{3.12}$$

From the definition given by equation (3.12) and the second assumption, vector $\mathbf{I}$ always lies on y axis. So vector $\mathbf{I}$ can be written as:

$$\mathbf{I} = I\hat{\mathbf{j}} \tag{3.13}$$

Then, based on these parameters which have been defined, the objective function in non-planar case can be formed. In order to rotate the angular momentum into z-axis, the rotate angle of angular momentum need to be close to vector $\mathbf{I}$. Due to equation (3.13), vector $\mathbf{I}$ has only one component on y-axis, then the rotate angle on other direction need to be zero. Then the objective functions Type *I* for non-planar case is formed as follow:

$$\min\left[w_1 \left(e_{GEO} - \hat{e} \right)^2 + w_2 \left(E_{GEO} - \hat{E} \right)^2 + w_3 (I - \hat{A}_y)^2 + w_4 (0 - \hat{A}_e)^2 \right] \tag{3.14}$$

where $\hat{A}_e$ is the angle accumulated over one revolution on the x-z plane. $\hat{A}_y$ is the angle accumulated over one revolution in the direction of y- axis.

And Type *II* is formed as:

$$\min\left[w_1 \left(h_{GEO} - \hat{h} \right)^2 + w_2 \left(E_{GEO} - \hat{E} \right)^2 + w_3 (I - \hat{A}_y)^2 + w_4 (0 - \hat{A}_e)^2 \right] \tag{3.15}$$

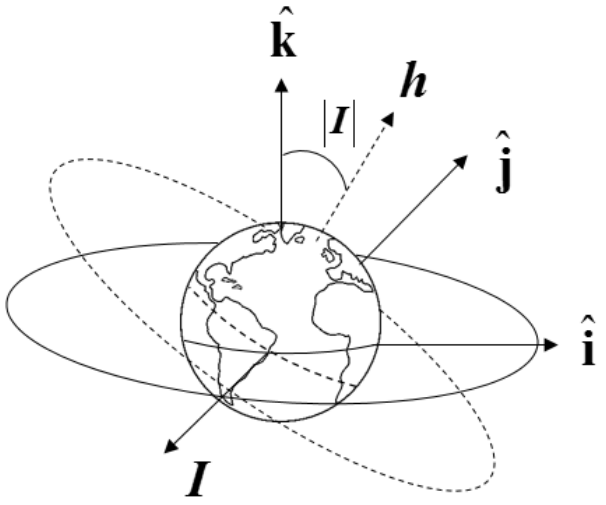

Figure 3.5 Graphical Definition of Vector $\boldsymbol{I}$

3.2.3 Direct Optimization Scheme

The direct optimization is performed over a single revolution. At the beginning, the current orbit or initial orbit will be divided into a small segments by the same size of true anomaly angle from $\theta_0 = 0$ to $\theta_n = 2\pi$ as shown in

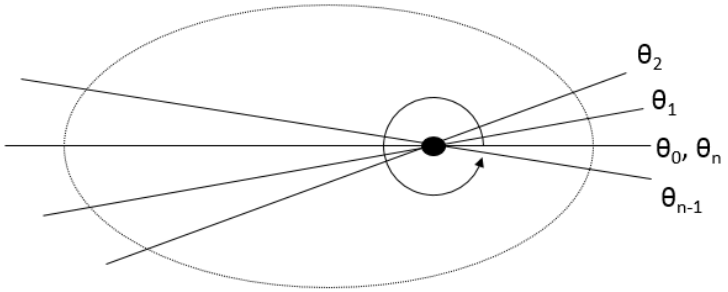

Figure 3.6 Segments of an orbit along true anomaly angle

The radius at each segment (r_j) can be calculated by the equation (2.15) by the initial value of total energy and angular momentum. Then, the radius at each segment is computed as below

$$r_j = \frac{h^2}{\mu + \sqrt{\mu^2 + 2Eh^2}\cos\theta_j} \text{ where } j = 0,1,...,n \tag{3.16}$$

Then numerical radius ($\tilde{r}_j$) for each segment is computed by the average of r_j at the edges so it can be calculated as follows:

$$\tilde{r}_j = \frac{r_{j-1} + r_j}{2} \text{ where } j = 1,2,...,n \tag{3.17}$$

After that, the numerical velocity ($\tilde{v}_j$) for each segment is computed by using the equation (2.3) as below.

$$\tilde{v}_j = \sqrt{\frac{2\mu}{\tilde{r}_j} + 2E} \text{ where } j = 1,2,...,n \tag{3.18}$$

The numerical time ($\tilde{t}_j$) which spacecraft spend at each segment is computed based on equation (2.12) so it is written as below

$$\tilde{t}_j = \frac{(r_{j-1})(r_j)\sin(\theta_j - \theta_{j-1})}{h} \text{ where } j = 1,2,...,n \tag{3.19}$$

After that, the flight path angle at each segment ($\tilde{\gamma}_j$) is calculated by equation (2.7):

$$\tilde{\gamma}_j = \begin{cases} \cos^{-1}\left(\frac{h}{\tilde{r}_j\tilde{v}_j}\right) & \text{if } \frac{(\theta_j + \theta_{j-1})}{2} \le \pi \\ -\cos^{-1}\left(\frac{h}{\tilde{r}_j\tilde{v}_j}\right) & \text{otherwise} \end{cases} \text{ where } j = 1,2,...,n \tag{3.20}$$

Due to presences of spacecraft in eclipses, the magnitude of the thrust is determined as below

$$\tilde{T}_j = \begin{cases} 0, & \text{if } \tilde{r}_j\cos\left(\frac{\theta_j + \theta_{j-1}}{2}\right) > 0 \quad \text{and} \quad \left|\tilde{r}_j\sin\left(\frac{\theta_j + \theta_{j-1}}{2}\right)\right| < r \\ T_{\max}, & \text{otherwise} \end{cases} \tag{3.21}$$

$$\text{where } j = 1,2,...,n$$

A. Planar Orbit-Raising Case

Due to presences of spacecraft in eclipses, the magnitude of the thrust is determined as below

$$\tilde{T}_j = \begin{cases} 0, & \text{if} \quad \tilde{r}_j \cos(\frac{\theta_j + \theta_{j-1}}{2}) > 0 \qquad \text{and} \qquad \left| \tilde{r}_j \sin(\frac{\theta_j + \theta_{j-1}}{2}) \right| < r \\ T_{\max}, & \text{otherwise} \end{cases} \tag{3.22}$$

$$\text{where} \quad j = 1, 2, ..., n$$

Due to the planar case, there is no components of the thrust which is out of the orbital plane. Then, the small change of total energy in each segment is approximately calculated by applying the equation (2.29):

$$\tilde{E}_j = \tilde{v}_j \frac{\tilde{T}_j}{m} \cos(\tilde{\gamma}_j + \alpha_j) \tilde{t}_j \quad \text{where} \quad j = 1, 2, ..., n \tag{3.23}$$

Also, the small change of angular momentum in each segment is approximately calculated by applying the equation (2.37)

$$\tilde{h}_j = \tilde{r}_j \frac{\tilde{T}_j}{m} \cos(\alpha_j) \tilde{t}_j \quad \text{where} \quad j = 1, 2, ..., n \tag{3.24}$$

At the end of the revolution, the total energy $\hat{E}$ and angular momentum $\hat{h}$ is the summation of the small changes within a revolution, so they can be expressed by

$$\hat{E} = E + \sum_{j=1}^{n} \tilde{E}_j \tag{3.25}$$

$$\hat{h} = h + \sum_{j=1}^{n} \hat{h}_j \tag{3.26}$$

In order to compute Type *I* objective function, the eccentricity at the end of revolution is computed by equation (2.14) as follows:

$$\hat{e} = \sqrt{1 + \frac{2\hat{E}\hat{h}^2}{\mu^2}} \tag{3.27}$$

At this point, the planar case problem can be solved by non-linear programming solver, fmincon in MATLAB®. Type *I* objective function is formed by substitute equation (3.25) and equation (3.26) into equation (3.9). Likewise, Type II objective function is formed by substitute equation (3.25) and equation (3.27) into equation (3.10). Once variable α_j is given by the solver, the next literature will be started with these $\hat{E}$ and $\hat{h}$ as initial value. The process for planar transfer is shown in

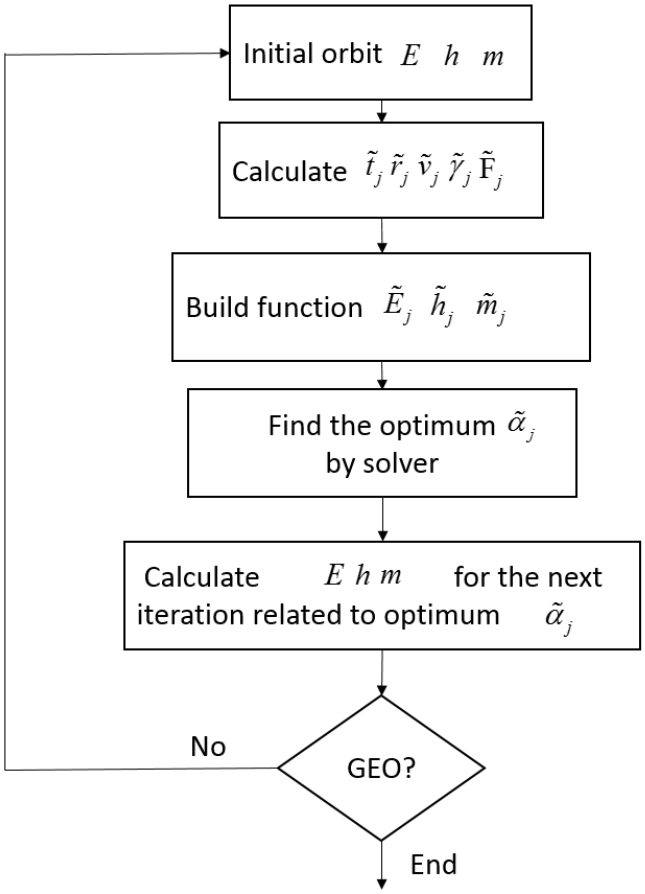

Figure 3.7 Flow chart of optimization process for planar case

B. Non-Planar Orbit-Raising Case

In non-planar case, the process is similar to planar case except the addition of orientation consideration. The angle β that defines the out-of-plane direction of the thrust is needed. From the definition of angle β which is given earlier and equation (3.23), the small change of total energy in each segment is computed by adding angle β in the formulation as below:

$$\tilde{E}_j = \tilde{v}_j \frac{\tilde{T}_j}{m} \cos(\tilde{\gamma}_j + \alpha_j) \cos(\beta_j) \tilde{t}_j \text{ where } j = 1, 2, ..., n \tag{3.28}$$

Likewise, the small change of angular momentum in each segment is computed as follows:

$$\tilde{h}_j = \tilde{r}_j \frac{\tilde{T}_j}{m} \cos(\alpha_j) \cos(\beta_j) \tilde{t}_j \text{ where } j = 1, 2, ..., n \tag{3.29}$$

Then, the total energy and angular momentum at the end of revolution can be obtained by equation (3.23) and (3.24), respectively. For Type I objective function, eccentricity can be obtain by equation (3.27).

For non-planar transfer, in order to align the orbit into the equatorial plane, the inclination has to be driven to zero. The equation (2.40), give the rotation direction of angular momentum vector due to the perturbation forces. As the matter of fact that angles can be considered as vectors, if these angles are the infinitesimal rotations or these angles are very small [26]. The angle that change in each segment is assumed to be small and can be computed as below.

$$\tilde{A}_{e,j} = \frac{\tilde{T}_j \tilde{r}_j}{mh} \sin(\beta_j) \cos(\frac{\theta_j + \theta_{j-1}}{2}) \tilde{t}_j \text{ where } j = 1, 2, ..., n \tag{3.30}$$

$$\tilde{A}_{y,j} = \frac{\tilde{T}_j \tilde{r}_j}{mh} \sin(\beta_j) \sin(\frac{\theta_j + \theta_{j-1}}{2}) \tilde{t}_j \text{ where } j = 1, 2, ..., n \tag{3.31}$$

where $\tilde{A}_{e,j}$ and $\tilde{A}_{p,j}$ the small angle that rotate in the direction of projections of x-axis and y-axis on the orbit plane ,respectively. The angle in equation (3.30) and (3.31) is assumed to be small, so the angle that change in one revolution is expressed as below:

$$\widehat{A}_e = \sum_{j=1}^{n} \tilde{A}_{e,j} \tag{3.32}$$

$$\widehat{A}_y = \sum_{j=1}^{n} \tilde{A}_{y,j} \tag{3.33}$$

In order to drive inclination angle to zero, $\widehat{A}_e$ is needed to be zero and $\widehat{A}_p$ is need to be equal to I which are described in equation (3.13). At this point, the non-planar case problem can be solved by non-linear programming solver.

CHAPTER 4

ALL-ELECTRIC ORBIT-RAISING SCENARIOS

The engine is selected to be BPT-4000 Hall thrusters because they are suitable for both small and large class of telecommunication satellites. For all scenarios, the four BPT-4000 thrusters are operated simultaneously. This is possible for large telecommunication satellites which has wide solar panels to provide the required power for the thrusters. The total thrust generated by these thrusters is 1.16 N at a specific impulse of 1788s. All the physical quantities are represented in non-dimensional units. The radius of GEO is defined as 1 distance unit (DU), whereas the time unit (TU) is such that Earth's gravitational constant is equal to 1 DU^3/TU^2. For the mass unit (MU), the initial mass of the spacecraft is defined to be equal to 1 MU.

The initial orbits for the problem are circular, elliptical and GTO. The same initial orbits are considered to investigate all scenarios. For the circular cases, the initial altitude are 1000, 3000, 5000, 10000, 16000 km. For the elliptical cases, all perigee of initial orbit is 220 km, the apogee are 10000, 20000, 30000, 40000 and 50000 km. For the GTO as initial orbits, the apogee is equal to altitude of GEO and the perigee are 4000, 6000, 8000 and 10000 km.

4.1 Trajectory Optimization without Eclipse Considerations in Planar Case

First, the transfer of a satellite is performed without the consideration of eclipses. In this case, the spacecraft continuously thrusts during the entire transfer. The results are determined with the two objective functions. The type *I* transfer use equation (3.9) as the objective function, and the type *II* use equation (3.10) as the objective function. The transfer times are shown in Table 4.1. In comparison of both transfers, the type *I* transfer show the shorter transfer times for all cases. The reason is that the apoapsis of trajectories in type *I* do not move far from the GEO. The apoapsis of trajectories in type II move far beyond GEO which means that the orbit period for a revolution is longer.

The trajectory of type *I* and type *II* are shown in Figure 4.1 and Figure 4.2, respectively. The initial orbit for both transfers is GTO with 10000 km perigee altitude. It is clearly seen that the apoapsis of transfer trajectory from type *II* moves further away beyond GEO than the apoapsis of transfer trajectory from type *I.* The reason is that the eccentricity in type *I* objective function induces the shape of trajectory as close to be circular shape as possible.

TABLE 4.1

TRANSFER TIME WITHOUT ECLIPSE CONSIDERATION IN PLANAR CASE

Initial Orbit		**Initial Mass (kg)**	**Transfer Time (days)**	
Perigee altitude (km)	***Apogee altitude (km)***		***Type II Transfer***	***Type I Transfer***
1000	1000	7300	286.11	279.19
3000	3000	7300	238.87	229.9
5000	5000	7300	200.99	193.35
10000	10000	4631	87.29	84.21
16000	16000	3173	38.69	37.86
220	10000	7300	227.59	214.46
220	20000	6716	183.5	164.73
220	30000	6485	167.31	146.87
220	40000	5974	149.68	128.1
220	50000	5640	142.5	118.75
4000	35786	4314	89.24	78.6
6000	35786	3873	73.7	65.25
8000	35786	3559	61.23	53.08
10000	35786	3319	55.18	45.2

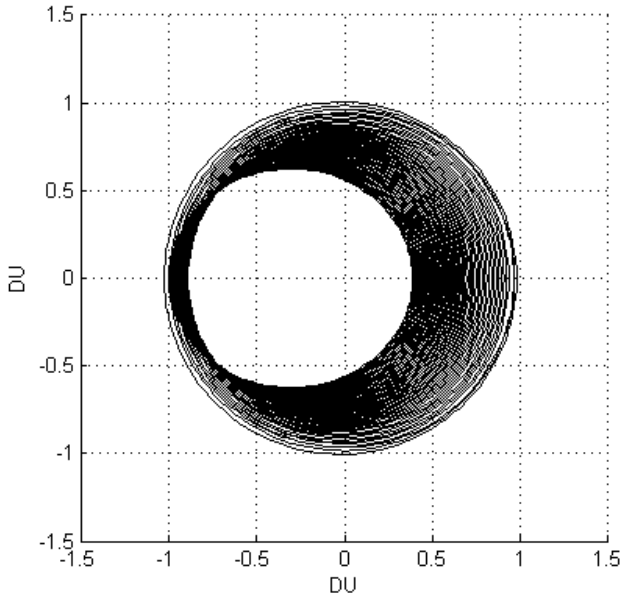

Figure 4.1 Type *I* transfer from GTO to GEO

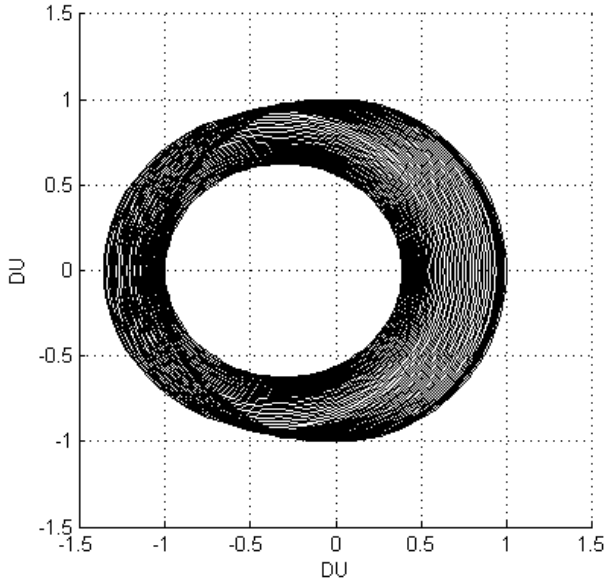

Figure 4.2 Type *II* transfer from GTO to GEO

4.2 Trajectory Optimization with Eclipse Considerations in Planar Case

In this section, the absence of the thrust due to eclipse is accounted for. All initial orbits are identical to previous cases. The results are generated from type I and type II transfers as shown in Table 4.2. The transfer times of eclipse consideration are longer than without eclipse consideration as expected. The transfer time, which is increased due to the effect of eclipse, is reduced by starting at higher altitude initial orbit.

The trajectories in Figure 4.3 and Figure 4.4 has the same initial orbit which is GTO with 10000 km periapsis altitude. For the eclipse consideration, the apoapsis of type *I* and type *II* move in the same trend as without eclipse consideration. For both types, there is an increase in transfer time compared to the without eclipse cases. The trend is such that, for the low altitude initial orbits the percentage increase in transfer time is high. But, for the high altitude initial orbit the percentage increase in transfer time is low. The reason is that at high altitudes, the time period of spacecraft in eclipse is comparatively low.

TABLE 4.2

TRANSFER TIME WITH ECLIPSE CONSIDERATION IN PLANAR CASE

Initial Orbit		**Initial Mass (kg)**	**Transfer Time (days)**		**% increase**	
Perigee altitude (km)	**Apogee altitude (km)**		**Type II Transfer**	**Type I Transfer**	**Type II Transfer**	**Type I Transfer**
1000	1000	7300	358.2	334.28	25.20	19.73
3000	3000	7300	278.69	263.53	16.67	14.63
5000	5000	7300	232.83	215.51	15.84	11.46
10000	10000	4631	111.16	91.02	27.35	8.09
16000	16000	3173	43.96	39.85	13.62	5.26
220	10000	7300	251.5	226.52	10.51	5.62
220	20000	6716	199.55	169.28	8.75	2.76
220	30000	6485	167.3	151.21	-0.01	2.95
220	40000	5974	138.83	132.74	-7.25	3.62
220	50000	5640	129.81	120.62	-8.91	1.57
4000	35786	4314	91.01	80.98	1.98	3.03
6000	35786	3873	79.76	66.16	8.22	1.39
8000	35786	3559	70.79	54.83	15.61	3.30
10000	35786	3319	58.6	45.75	6.20	1.22

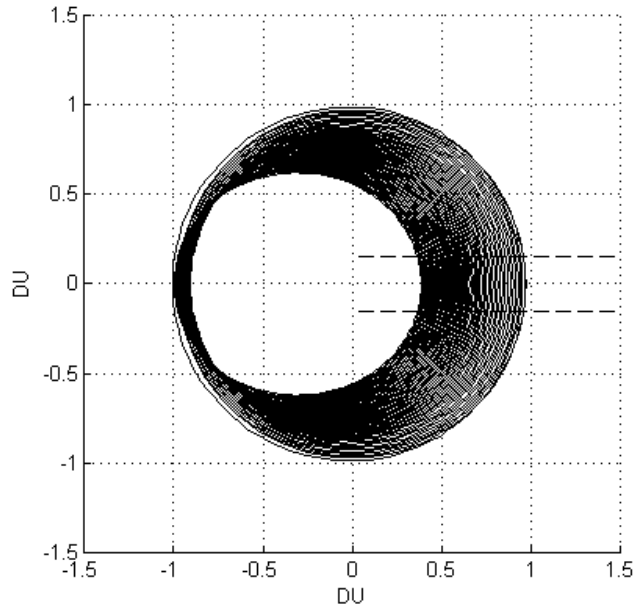

Figure 4.3 Type *I* transfer from GTO to GEO with eclipse consideration

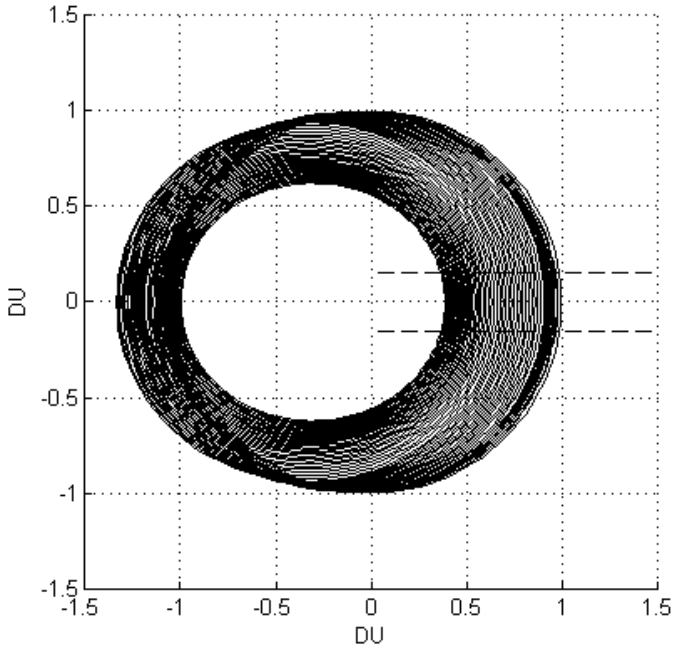

Figure 4.4 Type *II* transfer from GTO to GEO with eclipse consideration

4.3 Trajectory Optimization with Eclipse Considerations in Non-Planar Case

In this case, the initial orbit is not on the equatorial plane. The inclination angle of the initial orbit is not equal to zero. The transfer times of type II transfer are shown in TABLE 4.3.

TABLE 4.3

TRANSFER TIME WITH ECLIPSE CONSIDERATION IN NON-PLANAR CASE

Initial Orbit		**Inclination Angle (Degree)**	**Initial Mass (kg)**	**Transfer Time (days)**
Perigee altitude (km)	**Apogee altitude (km)**			**Type II Transfer**
1000	1000	28.5	8687	462.12
2000	2000	28.5	7085	358.32-
10000	35786	15	4392	81.56
20000	35786	15	3551	55.64
30000	35786	15	3130	44.74
10000	35786	28.5	7002	201.50
20000	35786	28.5	5471	147.40
30000	35786	28.5	4784	127.64

The trajectory of the case that has GTO as initial orbit with 30000 km altitude perigee and 28.5 inclination angle is shown in Figure 4.5. For clarity, Figure 4.6 and Figure 4.7 provide the projections of the trajectory on x-y plane and x-z plane, respectively.

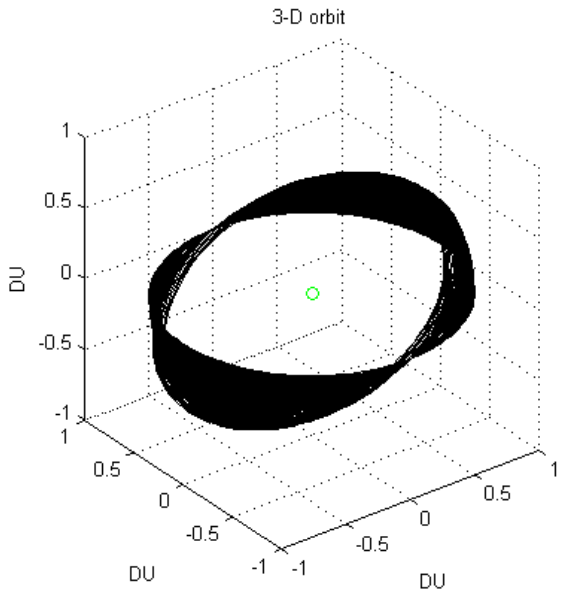

Figure 4.5 Type *II* transfer from GTO with inclination of 28.5 degree to GEO with eclipse consideration

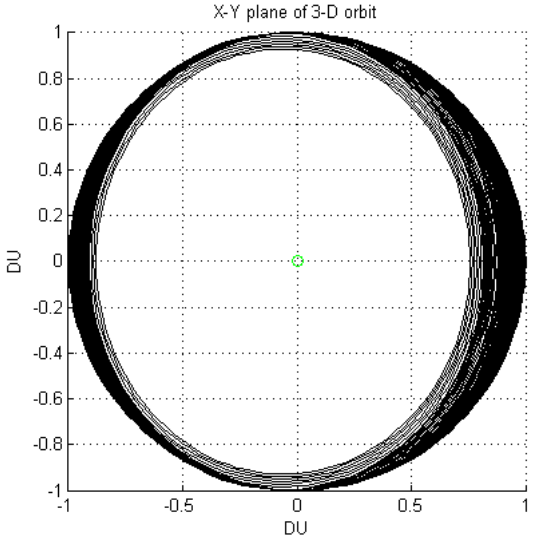

Figure 4.6 Projection of type *II* transfer from GTO with inclination of 28.5 degree to GEO on x-y plane with eclipse consideration

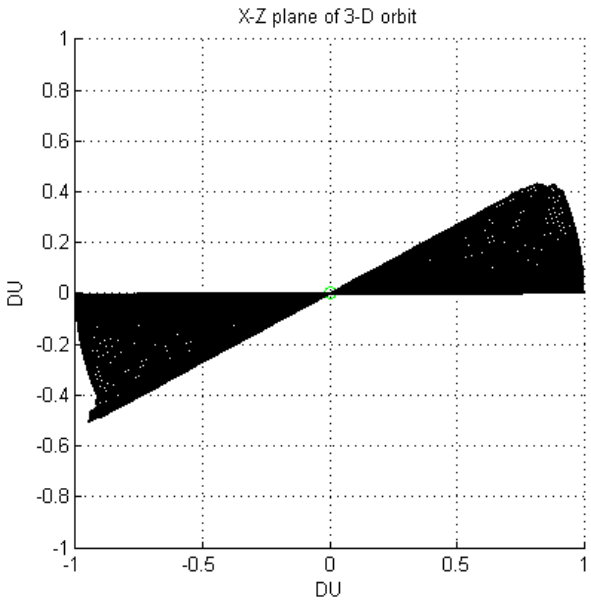

Figure 4.7 Projection of type *II* transfer from GTO with inclination of 28.5 degree to GEO on x-z plane with eclipse consideration

Additionally, the trajectory of the case that has the same initial orbit except that the inclination angle is equal to 15 is demonstrated in Figure 4.8. The projection of this trajectory on x-z plane is also shown in Figure 4.9.

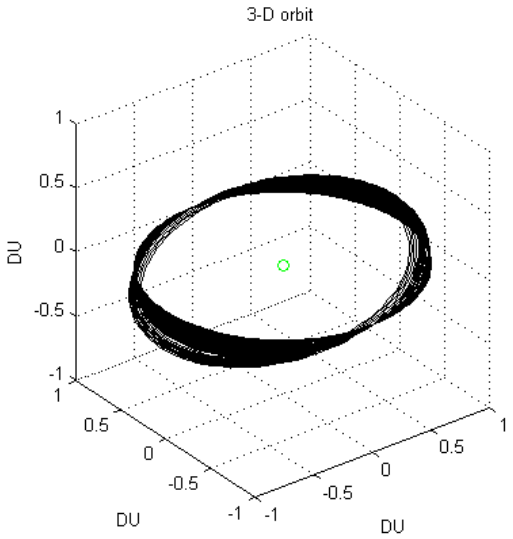

Figure 4.8 Type *II* transfer from GTO with inclination of 15 degree to GEO with eclipse consideration in 3D

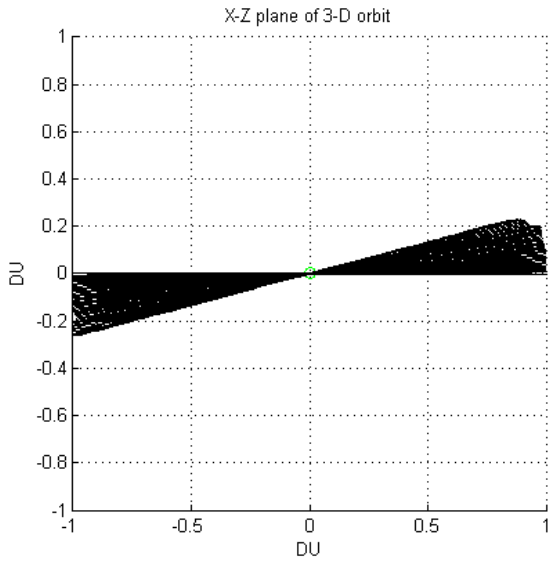

Figure 4.9 Projection of type *II* transfer from GTO with inclination of 15 degree to GEO on x-z plane with eclipse consideration

4.4 Trajectory Optimization with Switching Engine in Planar case

In order to reduce the exposure time to the radiation belts, the scenarios which the higer thrust is used, is analyzed. However, engine should be switched to the one that has more fuel saving after satellite goes beyond the radiation regions. In order to keep the same amount of satellite power, at the initial orbit, the engines are ten Arcjet thrusters each of which has a specific impulse of 502 s and thrust 0.254 N, and so the overall thrust is 2.54 N. When the perigee altitude reaches the switching altitude the engines are switched to 4 Hall thruster. The transfer time is calculated for all initial orbits at 3 switching altitudes 5000, 10000 and 15000 km as shown in Table 4.4.

Some initial orbits have the same transfer time for different switching altitudes because the initial orbit exceeds the switching altitude. The high switching altitude obviously gives a short transfer

time. The scenario of switching engines has advantages in term of reduction in exposure time to Van Allen belts by thrusting with higher magnitude in hazardous region.

TABLE 4.4

TRANSFER TIME OF ENGINE SWITCH SCENARIO

Initial Orbit		**Initial Mass (kg)**	**Transfer Time (day)**		
Perigee altitude (km)	**Apogee altitude (km)**		**5000 km**	**10000 km**	**15000 km**
1000	1000	7300	197.68	166.07	128.42
3000	3000	7300	194.86	148.95	123.04
5000	5000	7300	202.47	144.44	121.60
10000	10000	4631	101.95	100.04	66.83
16000	16000	3173	44.07	44.07	44.07
220	10000	7300	163.62	134.32	116.59
220	20000	6716	135.28	114.55	104.30
220	30000	6485	121.08	101.44	94.52
220	40000	5974	109.09	94.02	92.04
220	50000	5640	101.66	98.81	80.81
4000	35786	4314	77.28	66.37	67.50
6000	35786	3873	70.30	60.95	54.72
8000	35786	3559	59.85	56.46	45.11
10000	35786	3319	53.40	53.40	42.01

CHAPTER 5

CONCLUSION AND FUTURE WORK

All-electric satellites are now gaining favor among satellite manufacturers and operators of telecommunication satellites due to their significant benefits of fuel and cost savings. However, due to the low thrust of electric thrusters, the transfer to GEO takes significantly long time, thereby having several implications. From mission design point of view, obtaining the optimal trajectory for electric thrusters to the GEO is a complex problem, compared to a problem of chemical thrusters, taking into account the non-linear dynamics, eclipse constraints, provision of energy storage and solar array degradation. Also, long exposure to Van Allen radiation leads to radiation degradation of solar arrays along the path. Finally, electric orbit-raising represents a long waiting time for deploying satellites, so there are implications on the business aspect of satellite operators. This thesis presents a new algorithm to generate low-thrust trajectories suitable for use in mission analysis tools that aim to rapidly analyze multiple mission scenarios.

In order to obtain the solution, model of spacecraft dynamics around the Earth was analyzed by considering two-body problem and cylindrical shadow of the Earth. The rate of change of dynamical quantities are derived. These dynamical quantities are constants in the absence of non-gravitational forces, but change slowly in the presence of external forces. The low-thrust generated by the electric engines justifies the consideration of engine thrust as a perturbing force.

In the proposed technique, the long spiral trajectory of electric orbit-raising is broken into many parts, each comprised by a single revolution. Then, the optimal thrust profile is determined over a single revolution by using a direct optimization methodology. The objective function used is typical of a guidance-like scheme and minimizes the differences of dynamical quantities

between current states and the GEO. A sequence of such optimizations are carried out until the orbit can be considered to be GEO. The formulation is a combination of direct optimization and closed-loop guidance-like scheme.

The proposed methodology improves upon the work of Marasch and Hall [7] in the sense that it is applicable to any starting orbit. Ref. [7] methodology is suitable for planar circle-to-circle transfer only. The proposed formulation is not restricted to starting circular orbit. The initial orbit can be circular or elliptical. Moreover, the formulation of this method is capable of providing the solution for non-planar cases.

Two different objective types are considered. Type I transfer minimizes the deviation of total energy and eccentricity of final position from the GEO. Type II transfer minimizes the deviation of total energy and angular momentum of the final position from the GEO. The differences between trajectories from each type are illustrated in this thesis for several mission scenarios. The apoapsis of trajectory from type I does not deviate far from the GEO, but appoapsis of trajectory from type II does. The reason is that the eccentricity in type I objective explicitly forces the trajectory to be circular come at a faster rate. On the other, the parameters in type II do not. This difference leads to the transfer time of the type I being shorter because the trajectory does not go far from the Earth. The proposed methodology is also suitable for analyzing the engine types switch at some altitude. Such scenarios have never been investigated before and could potentially reduce transfer time by combining arcjet and Hall thruster, instead of just using Hall thrusters alone. Of course, this advantage comes at the cost of a mass penalty.

The proposed formulation does not have any singularity at GEO as Q-law [21, 22] does. Owing to this advantage, the final orbit achieved could be GEO. In contrast, the final orbit

obtained by using Q-law is often far from GEO and has an eccentricity of the order of 0.01 when starting from circular orbits, and of the order of 0.001 when starting from elliptic orbits.

Future extensions of this work are:

1. Consideration of energy storage to support thrusters in eclipses,
2. Use of Hermite–Simpson and more accurate discretization scheme instead of the trapezoidal discretization used in direct optimization,
3. Comprehensive mission scenario analysis using the developed tool to determine best deployment mechanism for all-electric satellites,
4. Application of the methodology in other orbital transfer problem, e.g. rendezvous problem

REFERENCES

REFERENCES

[1] Dutta, Atri, Libraro, Paola, Kasdin, Jeremy N. and Choueiri, Edgar, "A Direct Optimization Based Tool to Determine Orbit-Raising Trajectories to GEO for All-Electric Telecommunication Satellites," *AIAA/AAS Astrodynamics Specialist Conference*, Minneapolis, MN, 2012. **http://dx.doi.org/10.2514/6.2012-4589**

[2] Betts, John T., "Survey of Numerical Methods for Trajectory Optimization," *Journal of Guidance, Control, and Dynamics*, Vol. 21, No. 2, 1998, pp. 193-207.

[3] Conway, Bruce A., "A Survey of Methods Available for the Numerical Optimization of Continuous Dynamic Systems," *Journal of Optimization Theory and Applications*, Vol. 152, No. 2, 2012, pp. 271-306.

[4] Pontani, Mauro and Conway, Bruce A., "Optimal Low-Thrust Orbital Maneuvers via Indirect Swarming Method," *Journal of Optimization Theory and Applications*, Vol. 162, No. 1, 2014, pp. 272-292.

[5] Thorne, James D. and Hall, Christopher D., "Approximate initial Lagrange costates for continuous-thrust spacecraft," *Journal of Guidance, Control, and Dynamics*, Vol. 19, No. 2, 1996, pp. 283-288.

[6] Thorne, James D. and Hall, Christopher D., "Minimum-Time Continuous-Thrust Orbit Transfers Using the Kustaanheimo-Stiefel Transformation," *Journal of Guidance, Control, and Dynamics*, Vol. 20, No. 4, 1997, pp. 836-838.

[7] Marasch, Mark W. and Hall, D., "Application of Energy Storage to Solar Electric Propulsion Orbital Transfer," *Journal of Spacecraft and Rockets*, Vol. 37, No. 5, 2000, pp. 645-652.

[8] Gil, Philip E. , Murray, Walter and Saunder, Michael A. , "SNOPT: An SQP Algorithm for Large-Scale Constrained Optimization," *Society for Industrial and Applied Mathematics*, Vol. 47, No. 1, 2005, pp. 99-131.

[9] Wachter, Andreas and T., Biegler Lorenz, "On the implementation of an interior-point filter line-search algorithm for large-scale nonlinear programming," *Mathematical Programming*, Vol. 106, No. 1, 2005, pp. 25–57.

[10] Vanderbei, Robert J., "LOQO:an interior point code for quadratic programming," *Optimization Methods and Software*, Vol. 11, No. 1-4, 1999, pp. 451-484.

[11] Falck, Robert and Dankanich, John, "Optimization of Low-Thrust Spiral Trajectories by Collocation," *AIAA/AAS Astrodynamics Specialist Conference*, Minneapolis, MN, 2012. **http://dx.doi.org/10.2514/6.2012-4423**

REFERENCES (continued)

[12] Libraro, Paola, Kasdin, Jeremy N., Dutta, Atri and Choueiri, Edgar, "Application of a Quaternion-Based Formulation to the Electric Orbit-Raising of GEO Satellites from High-Inclination Injection Orbits," *AIAA/AAS Astrodynamics Specialist Conference*, San Diego, CA, 2014. **http://dx.doi.org/10.2514/6.2014-4426**

[13] Petropoulos, Anastassios E. and Longuski, James M., "Shape-Based Algorithm for the Automated Design of Low-Thrust, Gravity Assist Trajectories," *Journal of Spacecraft and Rockets*, Vol. 41, No. 5, 2004, pp. 787-796.

[14] Petropoulos, Anastassios E., "A shape-based approach to automated, low-thrust, gravity-assist trajectory design," Ph.D., Department of School of Aeronautics and Astronautics, Purdue University, Lafayette, IN, 2001.

[15] Vasile, M., Pascale, P. De and Casotto, S., "On the optimality of a shaped-based approach based on pseudo-equinoctial elements," *57th International Astronautical Congress*, 2006. **http://dx.doi.org/10.2514/6.IAC-06-C1.4.05**

[16] Bradley, Wall, "Shape-Based Approximation Method for Low-Thrust Trajectory Optimization," *AIAA/AAS Astrodynamics Specialist Conference and Exhibit*, Honolulu, Hawaii, 2008. **http://dx.doi.org/10.2514/6.2008-6616**

[17] Wall, Bradley J. and Conway, Bruce A., "Shape-Based Approach to Low-Thrust Rendezvous Trajectory Design," *Journal of Guidance, Control, and Dynamics*, Vol. 32, No. 1, 2009, pp. 95-101.

[18] Novak, D. M. and Vasile, M., "Improved Shaping Approach to the Preliminary Design of Low-Thrust Trajectories," *Journal of Guidance, Control, and Dynamics*, Vol. 34, No. 1, 2011, pp. 128-147.

[19] Abdelkhalik, Ossama and Taheri, Ehsan, "Shape Based Approximation of Constrained Low-Thrust Space Trajectories using Fourier Series," *Journal of Spacecraft and Rockets*, Vol. 49, No. 3, 2012, pp. 535-546.

[20] Kluever, Craig A., "Simple Guidance Scheme for Low-Thrust Orbit Transfers," *Journal of Guidance, Control, and Dynamics*, Vol. 21, No. 6, 1998, pp. 1015-1017.

[21] Petropoulos, Anastassios E., "Simple Control Laws for Low-Thrust Orbit," AIAA/AAS Astrodynamics Specialist Conference and Exhibit, Big Sky, MT, 2003.

[22] Petropoulos, Anastassios E., "Low-Thrust Orbit Transfers Using Candidate Lyapunov Functions with a Mechanism for Coasting," *AIAA/AAS Astrodynamics Specialist Conference and Exhibit*, Providence, RI, 2004. **http://dx.doi.org/10.2514/6.2004-5089**

REFERENCES (continued)

[23] Falck, Robert D., Sjauw, Waldy K. and Smith, David A., "Comparison of Low-Thrust Control Laws for Applications in Planetocentric Space," *50th AIAA/ASME/SAE/ASEE Joint Propulsion Conference*, Cleveland, OH, 2014. **http://dx.doi.org/10.2514/6.2014-3714**

[24] Prussing, John E. and Conway, Bruce A., *Orbital Mechanics*, 2 ed., Oxford University Press, 198 Madison Avenue, New York, NY 10016, 2012.

[25] Coordination, Inter-Agency Space Debris, "IADC Space Debris Mitigation Guidelines." 1 ed. Vol. 22.4, German Aerospace Center, September 2007.

[26] Kleppner, Daniel and Kolenkow, Robert J., *An Introduction to Mechanics*, Cambridge University Press, Cambridge, UK, 2010.